HHS Public Access

Author manuscript

Gastroenterology. Author manuscript; available in PMC 2024 December 01.

Published in final edited form as:

Gastroenterology. 2023 December ; 165(6): 1458–1474. doi:10.1053/j.gastro.2023.08.009.

HIF1A stabilization restores epigenetic control of *Nos1* expression and reverses gastroparesis in female diabetic mice

Fei Gao[1,2,3,10], **Yujiro Hayashi**[1,2], **Siva Arumugam Saravanaperumal**[1,2], **Gabriella B. Gajdos**[1,2], **Sabriya A. Syed**[1,2,4,11], **Aditya V. Bhagwate**[5], **Zhenqing Ye**[5,12], **Jian Zhong**[6], **Yuebo Zhang**[1,2], **Egan L. Choi**[1,2], **Sergiy M. Kvasha**[1,2,13], **Jagneet Kaur**[1,2,14], **Brooke D. Paradise**[1,2,4,15], **Liang Cheng**[1,2,5,16], **Brandon W. Simone**[1,2,4,17], **Alec M. Wright**[1,18], **Todd A. Kellogg**[8], **Michael L. Kendrick**[8], **Travis J. McKenzie**[8], **Zhifu Sun**[5,6], **Huihuang Yan**[5,6], **Chuanhe Yu**[1,2,19], **Adil E. Bharucha**[9], **David R. Linden**[1], **Jeong-Heon Lee**[6,7], **Tamas Ordog**[1,2,6,*]

[1]Enteric NeuroScience Program and Department of Physiology and Biomedical Engineering, Mayo Clinic, Rochester, MN, USA

[2]Gastroenterology Research Unit, Division of Gastroenterology and Hepatology, Department of Medicine, Mayo Clinic, Rochester, MN, USA

[3]Department of Gastroenterology, First Affiliated Hospital of Jinan University, Guangzhou, Guangdong, China

[4]Mayo Clinic Graduate School of Biomedical Sciences, Mayo Clinic, Rochester, MN, USA

[5]Division of Computational Biology, Department of Quantitative Health Sciences, Mayo Clinic, Rochester, MN, USA

[*]**Correspondence:** Tamas Ordog, M.D., Mayo Clinic, Guggenheim 10, 200 1st Street SW, Rochester, MN 55905 USA. Email: ordog.tamas@mayo.edu, phone: (507) 538-3906, fax: (507) 255-6318.

Author Contributions: F.G. performed experiments, analyzed data, and drafted the manuscript. Y.H., S.A. Saravanaperumal, G.B.G., S.A. Syed, J.Z., Y.Z., S.M.K., J.K., B.D.P., B.W.S., and A.M.W. performed experiments. F.G., A.V.B., and Z.Y. performed bioinformatic analyses. E.L.C. performed experiments and computational image analysis. Z.S. and H.Y. supervised a part of the bioinformatic analysis and contributed to the interpretation of the results. T.A.K., M.L.K., and T.J.M. provided critical resources. L.C. and C.Y. contributed to the interpretation of the epigenomic analyses and provided conceptual advice. A.E.B. provided critical resources and funding. D.R.L. supervised the animal studies and contributed to the interpretation of the in vivo results. J.H.L. supervised the chromatin immunoprecipitation-sequencing experiments and contributed to the interpretation of the results. T.O. conceived and supervised the project, contributed to data analysis and interpretation, wrote and edited the final version of the manuscript, and secured funding. All authors have approved the final version of the manuscript.

Disclosures: The authors disclose no conflicts.

Transcript Profiling: The microarray and RNA-sequencing (RNA-seq) data generated in this study have been deposited in a public database (National Center for Biotechnology Information, U.S. National Library of Medicine Gene Expression Omnibus (GEO), https://www.ncbi.nlm.nih.gov/gds/) as part of SuperSeries GSE139483, SubSeries GSE199990 (microarray) and GSE139472 (RNA-seq).

Writing Assistance: Not applicable.

Data Transparency Statement: The microarray, RNA-seq, chromatin immunoprecipitation-sequencing (ChIP-seq), and chromosome conformation capture-sequencing (HiC) data generated in this study have been deposited in a public database (National Center for Biotechnology Information, U.S. National Library of Medicine Gene Expression Omnibus (GEO), https://www.ncbi.nlm.nih.gov/gds/) as part of SuperSeries GSE139483, SubSeries GSE199990 (microarray), GSE139472 (RNA-seq), GSE139477, GSE139478, GSE139479, and GSE139481 (ChIP-seq), and GSE139470 (HiC). Processed microarray and sequencing results and outputs of gene expression and epigenomic data analysis software packages have been provided in **Supplementary Data** files.

[6]Center for Individualized Medicine, Mayo Clinic, Rochester, MN, USA

[7]Division of Experimental Pathology and Laboratory Medicine, Department of Laboratory Medicine and Pathology, Mayo Clinic, Rochester, MN, USA

[8]Department of Surgery, Mayo Clinic, Rochester, MN, USA

[9]Division of Gastroenterology and Hepatology, Department of Medicine, Mayo Clinic, Rochester, MN, USA

[10]Present address: Brown Center for Immunotherapy, Indiana University School of Medicine, Indianapolis, IN, USA

[11]Present address: The Jackson Laboratory for Genomic Medicine, Farmington, CT, USA

[12]Present address: Greehey Children's Cancer Research Institute, University of Texas Health San Antonio; San Antonio, TX, USA

[13]Present address: Institute of Molecular Biology and Genetics, Kyiv, Ukraine

[14]Present address: St. George's University School of Medicine, University Centre, Grenada, West Indies

[15]Present address: Rion Health, Rochester, MN, USA

[16]Present address: Institute for Cancer Genetics, Columbia University, New York, NY, USA

[17]Present address: Center for Cellular Immunotherapy, University of Pennsylvania, Philadelphia, PA, USA

[18]Present address: Division of Genetics and Genomics, Boston Children's Hospital, Boston, MA, USA

[19]Present address: The Hormel Institute, University of Minnesota, Austin, MN, USA

Abstract

Background and Aims: While depletion of neuronal nitric oxide synthase (*NOS1*)-expressing neurons contributes to gastroparesis, stimulating nitrergic signaling is not an effective therapy. We investigated whether hypoxia-inducible factor 1α (HIF1A), which is activated by high O_2 consumption in central neurons, is a *Nos1* transcription factor in enteric neurons and whether stabilizing HIF1A reverses gastroparesis.

Methods: Streptozotocin-diabetic mice, human and mouse tissues, $NOS1^+$ mouse neuroblastoma cells, and isolated nitrergic neurons were studied. Gastric emptying of solids and volumes were determined by breath test and single-photon emission computed tomography, respectively. Gene expression was analyzed by RNA-sequencing, microarrays, immunoblotting, and immunofluorescence. Epigenetic assays included chromatin immunoprecipitation-sequencing (13 targets), chromosome conformation capture-sequencing, and reporter assays. Mechanistic studies utilized Cre-mediated recombination, RNA interference, and CRISPR-Cas9-mediated epigenome editing.

Results: HIF1A signaling from physiological intracellular hypoxia was active in mouse and human $NOS1^+$ myenteric neurons but reduced in diabetes. Deleting *Hif1a* in *Nos1*-expressing

neurons reduced NOS1 protein by 50–92% and delayed gastric emptying of solids in female but not male mice. Stabilizing HIF1A with FG-4592/roxadustat, which is approved for human use, restored NOS1 and reversed gastroparesis in female diabetic mice. In nitrergic neurons, HIF1A upregulated *Nos1* transcription by binding and activating proximal and distal *cis*-regulatory elements including newly discovered super-enhancers, facilitating RNA polymerase loading and pause-release, and by recruiting cohesin to loop anchors to alter chromosome topology.

Conclusion: Pharmacological HIF1A stabilization is a novel, translatable approach to restoring nitrergic signaling and treating diabetic gastroparesis. The newly recognized effects of HIF1A on chromosome topology may provide insights into physioxia- and ischemia-related organ function.

Lay Summary

This study identifies a transcription factor that is required for the normal production of the main inhibitory neurotransmitter in the gastrointestinal tract and demonstrates that increasing its levels using a drug that is already approved for humans can reverse diabetic gastroparesis in female mice.

Graphical Abstract

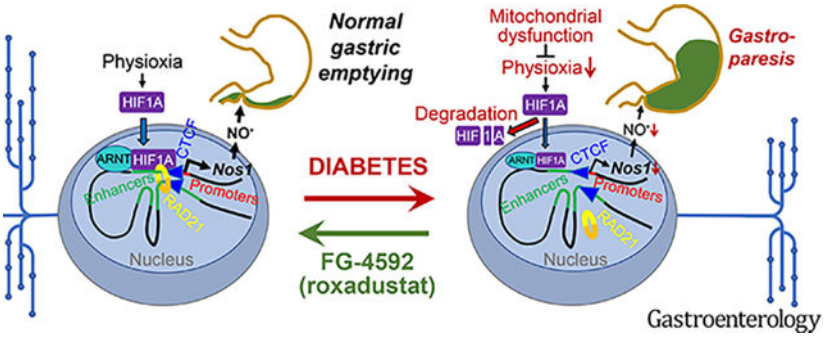

Keywords

physioxia; Hypoxyprobe; RAD21; CTCF

Introduction

Released by enteric neurons expressing neuronal nitric oxide synthase (NOS1), the inhibitory non-adrenergic, non-cholinergic neurotransmitter, nitric oxide (NO) regulates relaxation of the lower esophageal sphincter, gastric accommodation, and gastric emptying (GE).[1,2]

NOS1$^+$ neurons are preferentially depleted in gastroparesis (GP),[3–5] which is characterized by upper gastrointestinal symptoms and delayed GE without mechanical obstruction.[6] GP is approximately four times more common in women than men.[7] Delayed GE may be asymptomatic, accompanied by mild to moderate symptoms of dyspepsia, or with severe symptoms, nutritional compromise, anxiety, depression, and poor quality of life, which is referred to as gastroparesis.[7] GP is most frequently associated with and impairs glycemic control in diabetes mellitus (DM).[5,7] Loss of nitrergic neurons, due in part to repressed *Nos1* transcription,[8] has been causally linked to GP.[3,9,10] However, pharmacological stimulation of

nitrergic signaling also inhibits gastric contractility, facilitates storage rather than emptying, and can cause side effects.[6,11,12] Neuron transplantation[13,14] may have limited efficacy in DM due to the compromised tissue microenvironment. Therefore, we propose to restore nitrergic signaling by stimulating *Nos1* transcription in cells where *Nos1* is normally expressed. However, the mechanisms regulating *Nos1* expression are poorly understood.

Due to the high O_2 demands of oxidative phosphorylation (OXPHOS),[15] which energetically sustains synaptic functions, central neurons experience physiological hypoxia ("physioxia": partial O_2 tensions (pO_2) of 0.13–5.33 kPa or 0.13–5.26% O_2 at sea level[16]). These levels are sufficient to activate hypoxic signaling through the stabilization of hypoxia-inducible transcription factors (HIFs).[17–19] HIFs consist of a shared β subunit (ARNT; aryl hydrocarbon receptor nuclear translocator) and one of the three α subunits, HIF1A, HIF2A (Entrez Gene: EPAS1), and HIF3A.[17–19] Although HIFs are constitutively expressed, at high pO_2, α subunits are targeted for proteasomal degradation ($t_{1/2}$~4–6 min[20]) by HIF prolyl hydroxylases (PHDs). HIF PHDs are inhibited at low pO_2, allowing the α subunits' stabilization ($t_{1/2}$~200 min[20]) and translocation to the nucleus, where they complex with ARNT and bind their target promoters and enhancers.[21] Pharmacological inhibition of HIF PHDs can upregulate HIF1A and its targets and increase neuronal survival.[22] The HIF1A-stabilizing drug FG-4592 (roxadustat) has been approved in many countries for the treatment of anemia from chronic kidney disease, where DM and GP also occur.[23] Since subphysiological hypoxia upregulates *Nos1* mRNA in the nodose ganglion, cerebellum,[24] and vascular smooth muscle cells,[25] *Nos3* (endothelial NOS) and *Nos2* (inducible NOS) are targets for HIF1A,[26] and mitochondrial dysfunction and neuropathy are associated with delayed GE in DM,[27] we hypothesized that the neuronal transcriptional regulation of *Nos1* involves HIF1A, and that stabilizing HIF1A can restore NOS1 levels and correct GP.

Methods

Standard methods and additional details are described in the Supplementary Methods.

Human Tissues

Under the aegis of two protocols approved by the Mayo Clinic Institutional Review Board (IRB 13–008138 and 20–012002), gastric corpus tissues representing most of the greater curvature of the stomach were obtained from 7 female and 3 male nondiabetic (28–69 years of age) and 11 female diabetic patients (30–59 years of age) who underwent sleeve gastrectomy for obesity. Consent was obtained and recorded in the patients' electronic medical record.

Animal Studies

Animal experiments were performed in accordance with the National Institutes of Health Guide for the Care and Use of Laboratory Animals and ARRIVE guidelines (see Supplementary Methods). The protocols were approved by the Mayo Clinic Institutional Animal Care and Use Committee (A48315–15 and A2508–08). Except for the GE and gastric volume (GV) studies, which were performed in female mice, both male and female animals were used. None of the mice were used in unrelated experiments. Littermates were

used as controls. Before GE and GV tests, mice were fasted overnight in a metabolic cage with free access to water. Animals were handled during the light phase and euthanized by CO_2 inhalation or by decapitation performed under deep isoflurane (Baxter Healthcare, Deerfield, IL) inhalation anesthesia.

The following mouse strains were used (all from The Jackson Laboratory, Bar Harbor, ME): C57BL/6J; B6.129-*Hif1a*^{tm3Rsjo}/J (*Hif1a*^{fl}) mice, which have *loxP* sites flanking exon 2 of *Hif1a*; *Mapt*$^{tm1(EGFP)Klt}$/J (*Mapt*-EGFP) mice, which carry *EGFP* (enhanced green fluorescent protein) knocked in the first exon of the microtubule-associated protein tau (*Mapt*) gene; B6.129-*Nos1*$^{tm1(cre)Mgmj}$/J (*Nos1*^{cre}) mice, which express Cre recombinase from the 3' untranslated region of *Nos1*; and B6;129S-*Nos1*$^{tm1.1(cre/ERT2)Zjh}$/J (*Nos1*$^{creERT2/+}$) mice, which express CreERT2 fusion protein from the *Nos1* promoter/enhancer elements. Mice expressing switchable, membrane- or nucleus-targeted tandem dimer Tomato-EGFP constructs (*Gt(ROSA)26Sor*$^{tm4(ACTB-tdTomato,-EGFP)Luo}$/J (*R26*^{mTmG}) and B6;129S6-*Gt(ROSA)26Sor*$^{tm1(CAG-tdTomato*,-EGFP*)Ees}$/J (*R26*^{nTnG}), respectively) were used as reporters. In *Nos1*^{cre} mice, recombination occurred not only in NOS1^{+} myenteric neurons but also in NOS1^{-} cells (Supplementary Figure 2C), possibly due to germline recombination.[28] Since recombination in *Nos1*$^{creERT2/+}$ mice was limited to NOS1^{+} neurons, we used this strain for the conditional deletion of *Hif1a*.

To label hypoxic cells, mice were injected with 60 mg/kg pimonidazole (Hypoxyprobe™; Hypoxyprobe, Inc. Burlington, MA), which forms immunohistochemically detectable adducts with cellular proteins at pO_2<1.33 kPa (<0.28% O_2), intraperitoneally 60 min prior to euthanasia.[29] Cre-mediated recombination was induced with tamoxifen (Sigma-Aldrich, St. Louis, MO; 0.075 mg/g body weight intraperitoneally once daily for 3–5 days). Induction, monitoring, and management of streptozotocin diabetes was performed using published methods.[30]

GE of solids was determined by our previously published ^{13}C-octanoic acid breath test.[30,31] In female and male *Nos1*$^{creERT2/+}$;*Hif1a*$^{fl/fl}$ mice, 2 weekly GE $t_{1/2}$ values were averaged before and after tamoxifen or vehicle treatment. In female streptozotocin-diabetic mice, weekly measurements were taken (Supplementary Methods). Animals with two consecutive delayed GE readings (>97.5th percentile from 144 tests in 72 nondiabetic C57BL/6J females or from 120 tests in 60 nondiabetic C57BL/6J males) were considered to have GP.[32] Female diabetic mice with our without GP were treated with FG-4592 (roxadustat; 10 mg/kg intraperitoneally once daily for 4 weeks)[33] or vehicle (DMSO:PBS 1:49) for 4 weeks. The GE $t_{1/2}$ values obtained during the last 3 weeks of the treatment were averaged for each mouse. GVs were measured noninvasively by single-photon emission computed tomography (SPECT)[34] using intraperitoneally injected ^{99m}Tc-pertechnetate (100 μCi/50 μl) (Supplementary Figure 6A, Supplementary Videos 1–2) under isoflurane anesthesia.

Statistical Analysis

Hypothesis testing on low-throughput data was performed with GraphPad Prism 9.5.1 (Dotmatics, Boston, MA, USA) or SigmaPlot 14.5 (SPSS, Chicago, IL, USA) using nonparametric or parametric tests as appropriate (see Supplementary Methods). *P* values are exact values except in the case of Kruskal-Wallis ANOVA on ranks, where approximate

P values were computed. For high-throughput data, *P* values adjusted for false discovery rate (FDR) are reported as *Q* values.

Results

HIF1A is required for normal NOS1 protein levels and normal gastric emptying in female mice

We assessed hypoxia-related gene expression by Gene Set Enrichment Analysis (GSEA) in Affymetrix Mouse Genome 430.2 microarray data generated in-house from colonic *Mapt*-EGFP$^+$ neurons (Supplementary Figure 1A, Supplementary Data 1), total RNA-sequencing (RNA-seq) results from duodenal, ileal, and colonic *Phox2b*-CFP$^+$ neurons,[35] and single-cell RNA-seq data from small intestinal *Baf53b*-Tom$^+$ neurons (all clusters).[36] Using a matrix created by searching the Molecular Signatures Database (MSigDB) v.7.4 for neuronal or neurodegenerative disease-related gene sets containing *Nos1* (*Nos1*&Neuron; Supplementary Data 2) we first verified the strong representation of nitrergic neurons in these datasets (Supplementary Figure 1B–C, Supplementary Data 3). GSEA using the MSigDB Hallmark v.7.4 matrix revealed a significant enrichment of the Hypoxia and OXPHOS gene sets in all preparations and the Glycolysis gene set in all but the *Baf53b*-Tom$^+$ neurons (Figure 1A, Supplementary Figure 1D–E, Supplementary Data 3).

In the stomach of Hypoxyprobe™-injected mice, we detected intracellular hypoxia in luminal epithelial cells[29] and in mesothelial cells, KIT$^-$ interstitial cells, and myenteric (including nitrergic) neurons (Figure 1B, Supplementary Figure 2A). In gastric corpus tissues from nondiabetic patients, using two different antibodies we found overall stronger and even nuclear HIF1A staining in myenteric ganglion cells including nitrergic neurons than in non-neuronal cells (Figure 1C, Supplementary Figure 2B. Deleting *Hif1a* in *Nos1*$^{creERT2/+}$ mice, where tamoxifen treatment recombined 2 reporter constructs specifically and with ~70% efficiency (Supplementary Figure 2C), led to a 50% (stomach), 92% (small intestines), and 69% (proximal colon) reduction in median NOS1 protein levels 6 days post-tamoxifen and caused a delay in solid GE in females, with 50% showing gastroparetic GE $t_{1/2}$ values (Figure 1D). These results are nearly identical to the 48% prevalence of diabetic GP detected in females of the same background (see below). In male mice, which we found resistant to diabetic GP in a recent unpublished study (n=14), GE remained unaffected (Supplementary Figure 2D).

These results show that OXPHOS-driven intracellular hypoxia is prevalent and HIF1A signaling is active in NOS1$^+$ myenteric neurons. Our data also indicate that HIF1A is required for normal NOS1 levels and, in females, for normal GE.

Diabetes reduces HIF1A in NOS1$^+$ gastric myenteric neurons

Twelve weeks after the onset of diabetes in streptozotocin (STZ)-diabetic mice, Hypoxyprobe™ injection identified a substantial loss of physioxia in gastric myenteric ganglia, but no effect on the environmentally determined hypoxia in the epithelium (Figure 1E, **top**). In diabetic patients, HIF1A immunofluorescence was reduced in myenteric (including nitrergic) neurons of the gastric corpus (Fig. 1E, **middle**). Quantitative image

analysis (Supplementary Figure 3) revealed a direct linear relationship between HIF1A and NOS1 immunofluorescence and reduced HIF1A in nitrergic neurons of diabetic patients (Fig. 1E, **bottom**). These findings support our hypothesis that nitrergic enteric neuropathy in DM may arise from impaired hypoxic signaling.

HIF1A stabilization restores physioxic control of NOS1 and reverses diabetic gastroparesis

First, we validated the mouse neuroblastoma line N1E-115[37] for our studies. GSEA of total RNA-seq data (Supplementary Data 4) indicated enrichment of *Nos1*- and hypoxia-related gene sets in cells cultured for ≥3 days at either 20% or 4% O_2 (Supplementary Figure 4, Supplementary Data 5). Together with the (weak) nuclear HIF1A protein levels in cells maintained at 20% O_2 (Fig. 2A, Supplementary Figure 5A), these findings indicate that cellular metabolism is an important driver of intracellular hypoxia in N1E-115 cells.[15]

Environmental hypoxia approximating physiological O_2 in postcapillary tissues (4% O_2)[16] increased the expression of hypoxia-related genes and *Nos1* (Supplementary Figure 5B–C), the representation of *Nos1*-related gene sets (Supplementary Figure 4C–D), and HIF1A and NOS1 proteins by immunoblotting and immunofluorescence using two different antibodies for HIF1A (Figure 2A, Supplementary Figure 5A, C). We also verified the upregulation of *Nos1* mRNA and NOS1 protein in the conditionally immortalized fetal enteric neuronal precursor cells IM-FEN[38] (Supplementary Figure 5C). QIAGEN ingenuity Pathway Analysis of the differentially expressed genes in N1E-115 cells also supported a strong link between hypoxic and nitrergic signaling as NOS1-related pathways and networks were robustly represented among canonical pathways and upstream regulators, as well as causal, disease-, biological function-, and toxicology-related networks (Supplementary Data 6, Supplementary Figure 5D–E).

Reducing HIF1A protein by RNA interference (RNAi) using small interfering (si) RNAs suppressed hypoxia (4% O_2)-induced upregulation of NOS1 protein (Figure 2A). Conversely, pharmacological stabilization of HIF1A with the proteasome inhibitor MG-132 and the clinically approved PHD inhibitor FG-4592 increased NOS1 (Figure 2B, Supplementary Figure 5F).

In our validated GP model,[30,32] 11/23 (48%) female STZ-diabetic C57BL/6J mice developed GP (Figure 2C). GP mice treated with vehicle for ≥4 weeks (DDV group: diabetic, delayed, vehicle-treated) remained gastroparetic and had lower HIF1A and NOS1 protein and higher GV results than vehicle-treated mice with normal pretreatment GE (DRV group: diabetic, GP-resistant, vehicle-treated) (Figure 2D–F, Supplementary Figure 6A–C). In GP mice, FG-4592 (DDD: diabetic, delayed, drug-treated) increased HIF1A and NOS1, significantly reduced GE $t_{1/2}$ from pretreatment levels and restored it to normal in 5 of 6 mice, and normalized GVs. Pretreatment GE $t_{1/2}$ values were not different between GP or GP-resistant mice randomly assigned to FG-4592 or Veh treatment (Supplementary Figure 6D). Blood glucose did not differ among groups or correlate with GE $t_{1/2}$ (Supplementary Figure 6E).

These findings indicate that pharmacological stabilization of HIF1A can restore NOS1 protein levels and alleviate GP.

HIF1A binds promoters and enhancers of the *Nos1* locus

To understand how HIF1A regulates *Nos1* expression, we performed chromatin immunoprecipitation-sequencing (ChIP-seq) in N1E-115 cells cultured for 3 days at 20% or 4% O_2 (Supplementary Figures 7–8, Supplementary Data 7). HIF1A and ARNT binding was evident at 20% O_2, likely reflecting high O_2 consumption.[15] Culturing at 4% O_2 caused a robust increase in HIF1A and ARNT peak numbers, signals, and coincidence (Supplementary Figure 8A–B). Increased HIF1A and ARNT binding was detected near genes including established hypoxia-regulated genes in the KEGG "HIF-1 signaling pathway–Mus musculus" (mmu04066) pathway and the MSigDB Hallmark v.7.4 Hypoxia gene set (Supplementary Figure 8A, C and Supplementary Data 8) and was associated with increased gene expression (Figure 3A) including, in the case of HIF1A, of *Nos1*. Analysis of transcription factor binding motifs within the genomic footprints of the HIF1A and ARNT peaks in the vicinity of the KEGG mmu04066 genes indicated a robust representation of canonical HIF1A, EPAS1, and ARNT motifs, confirming the peaks' authenticity (Figure 3B, Supplementary Data 9). Consistent with the preference of HIF1A for promoters,[21] HIF1A binding sites located in promoters and exons increased at 4% O_2 (Supplementary Figure 8D). HIF1A and ARNT peaks were colocalized with the enhancer-associated histone mark monomethylated histone H3 lysine 4 (H3K4me1), the promoter-associated mark trimethylated H3K4 (H3K4me3), the active enhancer mark acetylated H3K27 (H3K27ac), and the active chromatin mark H3K9ac but not with the Polycomb-mediated repressive histone mark H3K27me3, indicating their predominant association with active chromatin (Figure 3C).

In the Ensembl *Nos1* locus (ENSMUSG00000029361), HIF1A and ARNT peaks were detected in three clusters with 3' ends located 0, 50, and 59 kb upstream of the transcription start site (TSS) of the nearest *Nos1* transcript encoding for a functional NOS1 isoform (*Nos1–206*, Figure 3D, Supplementary Figure 9A). Analysis of the binding profiles of key histone marks (Figure 3D), RNA polymerase II (POLR2), and POLR2 phosphorylated on serine 5 (POLR2S5p) or serine 2 (POLR2S2p) of its C-terminal repeat domain (Figure 4A, Supplementary Figure 9B), which are associated with transcriptional initiation, elongation, and termination,[39,40] together with epigenetic state modeling by ChromHMM (Supplementary Figure 8E) and enhancer/promoter reporter assays (Figure 3E) revealed the occurrence of these peaks within three cognate enhancer-promoter pairs (E1-P1, E2-P2, E3-P3). Except for P2, which, despite being occupied by initiating POLR2S5p (Figure 4A), had little H3K4me3 binding, all these *cis*-regulatory elements showed increased occupancy by their active histone marks in response to 4% O_2 (Figure 3D). We also observed prominent H3K4me3 occupancy of genomic sites corresponding to P1 and P3 in nitrergic neurons isolated from the small intestines of tamoxifen-treated $Nos1^{creERT2/+};R26^{mTmG}$ mice (Figure 3D, Supplementary Figure 8F). These results suggest a physiological role for the HIF-binding regulatory elements detected within the *Nos1* locus in the hypoxic control of *Nos1* expression.

HIF1A coordinates the activities of multiple *cis*-regulatory elements of the *Nos1* locus

StringTie2 assembly of total RNA-seq reads indicated that of the transcripts encoding for functional NOS1 isoforms (green fonts in the figures), *Nos1–206*, whose TSS maps

within P3, was most abundantly expressed and responsive to environmental hypoxia (Supplementary Figure 9A). While P1 included the TSSs of *Nos1–205*, which encodes for a truncated protein, and *Nos1–203*, a processed transcript, neither was expressed. We deleted P1 and P3 and also E1 using CRISPR-Cas9 in two N1E-115 clones each (Figure 4B, Supplementary Figure 9C, Supplementary Table 5) and analyzed *Nos1* expression using primers specific for the transcripts encoding for functional NOS1 and *Nos1–201*, a transcript subject to nonsense-mediated decay, which was not detectable (Supplementary Figure 9A). Deletion of E1 reduced *Nos1* expression at both 20% O_2 and 4% O_2 as did the deletion of P1 at 4% O_2, whereas deleting P3 had modest effects, possibly due to the incomplete elimination of the 3' end of the H3K4me3 peak (Supplementary Figure 9C). Chromosome conformation capture (3C) assays utilizing primers targeting genomic sites immediately upstream of E1 and P3 as "viewpoints" and target loci near the enhancers and promoters, flanking a binding site of the loop anchor/insulator CCCTC-binding factor (CTCF), and a control site (Figure 4C) revealed an interaction between E1-P1 and P3 at both 20% and 4% O_2 and short-range interactions between E1 and P1 and E3 and P3. There was a subtle shift from long-range to short-range interactions at 4% O_2, indicating that HIF1A binding may reinforce the interactions between cognate enhancers and promoters and suggesting a function for E1-P1 in stimulating *Nos1–206* expression beyond enhancing P3 activity through looping (Supplementary Figure 9D). Examining the RNA-seq data and ChIP-seq profiles for the transcriptional elongation-associated histone mark H3K36me3, POLR2, POLR2S5p, and POLR2S2p (Figure 4A) we noted the *Nos1* locus bore the characteristics of paused-and-expressed genes[40] with POLR2 and POLR2S5p accumulation at all 3 promoters, a sign of transcription initiation and pausing, and occupancy by POLR2S2p and H3K36me3 throughout the locus indicating elongation. All these signals increased in response to 4% O_2, consistent with HIF1A's role in facilitating transcriptional pause-release.[41] POLR2S2p also accumulated at sites with POLR2 and POLR2S5p peaks and having low H3K36me3 occupancy, suggesting a coincidence between transcription termination and initiation sites.[39,40] This is consistent with "preloading" of elongating POLR2 onto successive initiation sites, which could potentially result in more robust expression of *Nos1* encoding for functional NOS1 protein, particularly at low pO_2 (Supplementary Figure 9E).

HIF1A-binding remote super-enhancers interact with *cis*-regulatory elements of the *Nos1* locus

To discover new remote *cis*-regulatory elements controlling *Nos1* expression, we performed two independent chromosome conformation capture-sequencing (HiC) studies utilizing the Arima, Inc. 2-enzyme chemistry and a published HiC protocol[42] (Supplementary Figure 10A). Both localized *Nos1* within a 5' subdomain of an ~800 kb topologically associating domain (TAD) (Supplementary Figure 10B). Within this TAD we identified, using Rank Ordering of Super-Enhancers (ROSE), 2 (at 20% O_2) and 3 (at 4% O_2) HIF1A-bound super-enhancers (SEs) located 5' of the *Nos1* locus and one SE, which was detectable at both pO_2 levels, 3' of *Nos1* (Figure 5A). Using HiCCUPS we detected >30,600 unique loops (Supplementary Figure 10C, Supplementary Data 10). Chromosome-wise assessment of the enrichment of the HiC signal in loops by aggregate peak analysis (APA)[43] indicated concordant peak-to-lower-left (P2LL) enrichment values in the Arima and *Nco*I HiC data (Supplementary Figure 10D). The numbers of HiCCUPS loops and genome-wide APA

enrichment values were similar at 20% and 4% O_2 (Supplementary Figures 10C, E and 11A). Within the *Nos1*-containing subdomain, the Arima HiC data revealed 14 loops shared between the HiC matrices obtained at 20% O_2 and 4% O_2 and 6 and 7 loops that were unique to the 20% O_2 and 4% O_2 datasets, respectively (Figure 5A–C, Supplementary Data 11). Notably, the shared loops included the loop connecting E3 and the more distal *cis*-regulatory elements of the *Nos1* locus we previously identified by 3C (Figure 4C). Other notable changes included the replacement of a loop connecting E3 with the 3' SE at 20% O_2 with a loop between E3 and one of the 5' SEs and newly formed connections between E1 and E2 and upstream enhancers/SEs. Considering peaks of the loop anchor protein CTCF, the cohesin component RAD21, and the orientation of CTCF motifs at the 12 clusters of loop anchor sites,[44] we classified these loops as architectural (loops with significant, coincident RAD21 and CTCF peaks at both anchors, with CTCF peaks occupying motifs with convergent or left/right tandem configurations) or transient/functional (loops lacking one or more component or having a divergent CTCF motif orientation)[45] (Figure 5A–C). This analysis identified 6, 3, and 3 of the shared, 20% O_2-only, and 4% O_2-only loops, respectively, as architectural and revealed that culturing at 4% O_2 changed the loop connecting the *Nos1*-proximal E3 with a 5' SE from functional to architectural due to the recruitment of RAD21 to the CTCF peak at anchor site #3' (Figure 5B–C, Supplementary Figure 10F). These findings indicate that the *cis*-regulatory elements of the *Nos1* locus are coupled to remote SEs within its TAD in a pO_2-dependent manner and that the effects of environmental hypoxia involve substantial reconfiguration and strengthening of these interactions.

HIF1A alters chromosome topology genomewide

Besides a RAD21 peak, the loop anchor site #3' also gained a HIF1A peak at 4% O_2 (Supplementary Figure 10F). Within all 12 clusters of *Nos1*-relevant loop anchors, apart from the intra-*Nos1* anchor #9, HIF1A binding coinciding with RAD21 and CTCF peaks increased at low pO_2 (Figure 6A). The pO_2-dependent concordance among CTCF, RAD21, and HIF1A peaks was also evident genome-wide (Figure 6B) including within loop anchors (Figure 6C–D) and accompanied by an increase in the number of overlapping HIF1A, RAD21, and CTCF peaks at 4% O_2 (Figure 6E). ChromHMM analysis using all ChIP-seq data (Supplementary Figure 11B–C) identified an active distal enhancer and an active promoter state (states 11 and 12, respectively) that had the strongest HIF1A and ARNT enrichment among all states and could be classified as loop anchor-associated. Analysis of chromatin state changes by Sankey plot (Figure 6F) revealed an expansion of these states at the expense of enhancers and promoters not associated with chromosome loops (states 9 and 13). These results suggest that the conversion of a functional loop to architectural in the *Nos1* TAD reflected genome-wide actions of HIF1A stabilization and recruitment.

HIF1A recruits RAD21 to CTCF-bound sites to upregulate NOS1

Considering that low pO_2 affected CTCF binding less than HIF1A and RAD21 occupancy and neither *Rad21* nor *Ctcf* expression was modified by pO_2 (Supplementary Data 4), we investigated whether HIF1A could regulate chromosome conformation by binding to CTCF and recruiting RAD21. Consistent with the ability of HIF1A to bind noncanonical motifs,[46] we detected enrichment of CTCF motifs within the HIF1A-bound *cis*-regulatory elements

of the *Nos1*-containing sub-TAD (Figure 7A, Supplementary Data 12). RAD21 and HIF1A co-immunoprecipitation with CTCF and RAD21 verified HIF1A binding to both CTCF and RAD21 along with RAD21-CTCF binding (Figure 7B). At 4% O_2, RNAi-mediated depletion of HIF1A binding within key enhancers/SEs of the *Nos1*-containing sub-TAD (Supplementary Figure 11D) and the promoter of the HIF1A target *Slc2a1* (dotted pink line in Supplementary Figure 8A) also caused the reduction of RAD21 binding to the same sites (Figure 7C). RNAi-mediated depletion of RAD21 inhibited the hypoxia-induced gain in NOS1 protein and reduced NOS1 at 20% O_2 (Figure 7D). Together, these results indicate that besides upregulating enhancer/promoter activities, HIF1A facilitates enhancer-promoter interactions by binding to CTCF sites and promoting the formation of architectural chromosome loops by the recruitment of RAD21 (Figure 7E).

Discussion

While NOS1 is central to GP,[3,4,9,10] supplementing NO via pharmacotherapy is ineffective,[6,11,12] and transplantation of nitrergic neurons[13,14] may have limited efficacy in DM due to the compromised tissue microenvironment. Here, we demonstrate that HIF1A is required to maintain normal NOS1 levels and, in female mice, also GE. Conceivably, this may explain the poorly understood finding that over 65% of patients with diabetic GP are women.[7] We also observed that diabetes reduces hypoxia/HIF1A in $NOS1^+$ gastric myenteric neurons in mice and humans. FG-4592/roxadustat, which has been used in chronic kidney disease patients,[23] stabilized HIF1A, reversed the downregulation of NOS1 protein, and restored GE in female diabetic mice (Figure 7F). Besides stimulating gene expression by binding to promoter-proximal elements,[21] we also found HIF1A to upregulate transcription from the 5' end of the *Nos1* locus to increase the number of POLR2 complexes available at the TSS of the main *Nos1* transcript encoding for functional NOS1 protein. Finally, we demonstrate that HIF1A facilitates long-range enhancer/SE-promoter interactions by altering chromosome topology through the recruitment of cohesin to CTCF-bound sites within the *Nos1* TAD and genomewide. The recognition of HIF1A's role in 3D chromosome conformation may lead to better understanding of organ functions at physioxia and in ischemic conditions[47] and the pathobiology of cancers.[17–19]

In enteric neurons, hypoxic signaling is activated under physiological conditions, likely reflecting high oxygen consumption.[15,16] This physioxic signaling, also evident in N1E-115 cells, was reduced in diabetic mice and humans. These findings are consistent with the association of DM-associated mitochondrial dysfunction with neuropathy and delayed GE.[27] High oxidative stress from downregulation of macrophage heme oxygenase-1[32] may also contribute to the impaired expression and function of HIF1A in DM.[19] Stabilizing HIF1A normalized GE and GVs in diabetic mice, reflecting a robust stimulation of NOS1. Indeed, NOS1 was more sensitive to HIF1A in diabetic mice with vs. without GP. This may have reflected reduced production of NO in GP, which at high concentrations can inhibit HIF1A function.[19] We did not study HIF1A/EPAS1 or HIF3A, which are not expressed by N1E115 cells, but they may have contributed to the effects of FG-4592 in mice. Stabilizing HIFs may also enhance the function of transplanted nitrergic neurons.[14] Arguably, hypobaric hypoxia or carbon monoxide-releasing molecules (CORMs) may have effects similar to FG-4592.[48]

However, hypobaric hypoxia therapy has practical limitations, and CORMs may aggravate mitochondrial dysfunction by disabling cytochromes.[48]

Akin to mice with targeted disruption of *Nos1*,[9] the stomach was larger in diabetic mice, arguably due to pyloric dysfunction and functional gastric outlet obstruction secondary to reduced *Nos1* expression.[6] In these mice, FG-4592 *reduced* gastric volume, which contrasts with the pan-gastric relaxation of drugs that upregulate NO levels in humans.[6,11,12] Although interstitial cells of Cajal, whose depletion contributes to GP,[6,49] are not naturally hypoxic (Supplementary Figure 2A), their numbers could be increased/normalized by the restoration of NO signaling with FG-4592.[50]

We also discovered 4 pO_2-regulated SEs within the *Nos1* TAD. These SEs are more strongly coupled to proximal *Nos1* enhancers under physioxia. These interactions included de-novo transient loops, reorganization of architectural loops, and the conversion of a transient to an architectural loop, with the latter involving recruitment of HIF1A and RAD21 to an existing CTCF peak. Evident throughout the genome, these findings are consistent with the model that physioxia leads to HIF1A-directed formation of cohesin-mediated, CTCF-delimited architectural loops. In DM, there is less intracellular hypoxia and these interactions dissolve (Figure 7E). Future studies will address whether the HIF1A-RAD21 interactions involve other members of the cohesin complex and whether HIF1A interacts with transcription factors important for the specification of the NOS1 neuronal lineage such as *Etv1*[36] to limit HIF1A-mediated *Nos1* upregulation to nitrergic neurons.

Supplementary Material

Refer to Web version on PubMed Central for supplementary material.

Acknowledgements:

The authors thank Dr. Shanthi Srinivasan, Emory University, Atlanta, Georgia, USA, for her generous gift of the conditionally immortalized mouse IM-FEN cells line; Teresa D. Decklever (Small Animal Imaging Core, Mayo Clinic, Rochester, MN, USA) for the gastric volume measurements; Natalie R. Wertish (Enteric NeuroScience Program and Department of Physiology and Biomedical Engineering, Mayo Clinic, Rochester, MN, USA) for her assistance with the gastric emptying tests; the Center for Individualized Medicine Medical Genome Facility (Mayo Clinic, Rochester, MN, USA) for the next-generation sequencing; and Pritha Chanana, Krutika S. Gaonkar, Gavin R. Oliver (Center for Individualized Medicine Bioinformatics Core and Division of Computational Biology, Department of Quantitative Health Sciences, Mayo Clinic, Rochester, MN, USA) for their contribution to the bioinformatic analyses.

Grant Support:

This study was supported in part by National Institutes of Health grants R01 DK126827, R01 DK131455, P01 DK068055, P30 DK084567, and the Mayo Clinic Center for Individualized Medicine. The funding agencies had no role in the study analysis or writing of the manuscript. Its contents are solely the responsibility of the authors.

Abbreviations:

3C	chromosome conformation capture
APA	aggregate peak analysis
ARNT	aryl hydrocarbon receptor nuclear translocator

BAC	bacterial artificial chromosome
BAF53B	alias of ACTL6B, actin-like 6B
CFP	cyan fluorescent protein
ChIP-seq	chromatin immunoprecipitation-sequencing
CORM	carbon monoxide-releasing molecule
CM	circular muscle
CTCF	CCCTC-binding factor
CTD	C-terminal repeat domain
DAPI	4’,6-diamidino-2-phenylindole
DB	differential binding
DDD	diabetic, delayed gastric emptying, FG-4592-treated
DDV	diabetic, delayed gastric emptying, vehicle-treated
DM	diabetes mellitus
DRD	diabetic, resistant to gastroparesis, FG-4592-treated
DRV	diabetic, resistant to gastroparesis, vehicle-treated
E	enhancer
EGFP	enhanced green fluorescent protein
EPAS1	endothelial PAS domain protein 1 (alias: HIF2A)
FACS	fluorescence-activated cell sorting
FDR	false discovery rate
GE	gastric emptying
GP	gastroparesis
GSEA	Gene Set Enrichment Analysis
GV	gastric volume
H3K27ac	acetylated histone H3 lysine 27
H3K27me3	trimethylated histone H3 lysine 27
H3K36me3	trimethylated histone H3 lysine 36
H3K4me1	monomethylated histone H3 lysine 4
H3K4me3	trimethylated histone H3 lysine 4

H3K9ac	acetylated histone H3 lysine 9
HiC	chromosome conformation capture-sequencing
HIF	hypoxia-inducible factor
HIF1A	hypoxia inducible factor 1, α subunit
HP	Hypoxyprobe™
HuC/D	alias of ELAV like neuron-specific RNA binding protein 3 and ELAV like RNA binding protein 4
IC	interstitial cell
IM-FEN	immortalized fetal enteric neuron
LM	longitudinal muscle
MAPT	microtubule-associated protein tau
Mes	mesothelial cell
MSigDB	Molecular Signatures Database
Muc	mucosa
ND	nondiabetic
NO	nitric oxide
NOS1	nitric oxide synthase 1, neuronal
NOS2	nitric oxide synthase 2, inducible
NOS3	nitric oxide synthase 3, endothelial cell
OXPHOS	oxidative phosphorylation
P	promoter
P2LL	peak to lower left quadrant
PHD	prolyl hydroxylase domain
PHOX2B	paired-like homeobox 2b
pO_2	partial oxygen tension
POLR2	RNA polymerase II
POLR2S2p	RNA polymerase II phosphorylated on C-terminal repeat domain serine 2
POLR2S5p	RNA polymerase II phosphorylated on C-terminal repeat domain serine 5

R26	ROSA26 locus
RAD21	RAD21 cohesin complex component
RCF	relative crosslinking frequency
RNAi	RNA interference
RNA-seq	RNA-sequencing
Scr	scrambled
SE	super-enhancer
siRNA	small interfering RNA
SLC2A1	solute carrier family 2 (facilitated glucose transporter), member 1 (alias: GLUT1)
SPECT	single-photon emission computed tomography
STZ	streptozotocin
TAD	topologically associating domain
Tam	tamoxifen
Tom	Tomato fluorescent protein
TSS	transcription start site
TUBB3	tubulin, beta 3 class III
UCHL1	ubiquitin carboxy-terminal hydrolase L1
Veh	vehicle

References

Author names in bold designate shared co-first authorship.

1. Rao M, Gershon MD. The bowel and beyond: the enteric nervous system in neurological disorders. Nat Rev Gastroenterol Hepatol 2016;13:517–528. [PubMed: 27435372]
2. Rivera LR, Poole DP, Thacker M, et al. The involvement of nitric oxide synthase neurons in enteric neuropathies. Neurogastroenterol Motil 2011;23:980–988. [PubMed: 21895878]
3. Watkins CC, Sawa A, Jaffrey S, et al. Insulin restores neuronal nitric oxide synthase expression and function that is lost in diabetic gastropathy. J Clin Invest 2000;106:373–384. [PubMed: 10930440]
4. Anitha M, Gondha C, Sutliff R, et al. GDNF rescues hyperglycemia-induced diabetic enteric neuropathy through activation of the PI3K/Akt pathway. J Clin Invest 2006;116:344–356. [PubMed: 16453021]
5. Grover M, Farrugia G, Lurken MS, et al. Cellular changes in diabetic and idiopathic gastroparesis. Gastroenterology 2011;140:1575–1585 e1578. [PubMed: 21300066]
6. Camilleri M, Sanders KM. Gastroparesis. Gastroenterology 2022;162:68–87 e61. [PubMed: 34717924]

7. Bharucha AE, Kudva YC, Prichard DO. Diabetic Gastroparesis. Endocr Rev 2019;40:1318–1352. [PubMed: 31081877]
8. Cellek S, Foxwell NA, Moncada S. Two phases of nitrergic neuropathy in streptozotocin-induced diabetic rats. Diabetes 2003;52:2353–2362. [PubMed: 12941776]
9. Huang PL, Dawson TM, Bredt DS, et al. Targeted disruption of the neuronal nitric oxide synthase gene. Cell 1993;75:1273–1286. [PubMed: 7505721]
10. Mashimo H, Kjellin A, Goyal RK. Gastric stasis in neuronal nitric oxide synthase-deficient knockout mice. Gastroenterology 2000;119:766–773. [PubMed: 10982771]
11. Bortolotti M, Mari C, Lopilato C, et al. Sildenafil inhibits gastroduodenal motility. Aliment Pharmacol Ther 2001;15:157–161. [PubMed: 11148432]
12. Dishy V, Cohen Pour M, Feldman L, et al. The effect of sildenafil on gastric emptying in patients with end-stage renal failure and symptoms of gastroparesis. Clin Pharmacol Ther 2004;76:281–286. [PubMed: 15371988]
13. Micci MA, Pasricha PJ. Neural stem cells for the treatment of disorders of the enteric nervous system: strategies and challenges. Dev Dyn 2007;236:33–43. [PubMed: 17029286]
14. Stavely R, Hotta R, Picard N, et al. Schwann cells in the subcutaneous adipose tissue have neurogenic potential and can be used for regenerative therapies. Sci Transl Med 2022;14:eabl8753. [PubMed: 35613280]
15. Sim J, Cowburn AS, Palazon A, et al. The Factor Inhibiting HIF Asparaginyl Hydroxylase Regulates Oxidative Metabolism and Accelerates Metabolic Adaptation to Hypoxia. Cell Metab 2018;27:898–913 e897. [PubMed: 29617647]
16. Erecinska M, Silver IA. Tissue oxygen tension and brain sensitivity to hypoxia. Respir Physiol 2001;128:263–276. [PubMed: 11718758]
17. Pugh CW, Ratcliffe PJ. New horizons in hypoxia signaling pathways. Exp Cell Res 2017;356:116–121. [PubMed: 28315322]
18. Ivan M, Kaelin WG Jr. The EGLN-HIF O2-Sensing System: Multiple Inputs and Feedbacks. Mol Cell 2017;66:772–779. [PubMed: 28622522]
19. Semenza GL. Regulation of mammalian O2 homeostasis by hypoxia-inducible factor 1. Annu Rev Cell Dev Biol 1999;15:551–578. [PubMed: 10611972]
20. Moroz E, Carlin S, Dyomina K, et al. Real-time imaging of HIF-1alpha stabilization and degradation. PLoS One 2009;4:e5077. [PubMed: 19347037]
21. Smythies JA, Sun M, Masson N, et al. Inherent DNA-binding specificities of the HIF-1alpha and HIF-2alpha transcription factors in chromatin. EMBO Rep 2019;20.
22. Li X, Cui XX, Chen YJ, et al. Therapeutic Potential of a Prolyl Hydroxylase Inhibitor FG-4592 for Parkinson's Diseases in Vitro and in Vivo: Regulation of Redox Biology and Mitochondrial Function. Front Aging Neurosci 2018;10:121. [PubMed: 29755339]
23. Chen N, Hao C, Liu BC, et al. Roxadustat Treatment for Anemia in Patients Undergoing Long-Term Dialysis. N Engl J Med 2019;381:1011–1022. [PubMed: 31340116]
24. Prabhakar NR, Pieramici SF, Premkumar DR, et al. Activation of nitric oxide synthase gene expression by hypoxia in central and peripheral neurons. Brain Res Mol Brain Res 1996;43:341–346. [PubMed: 9037552]
25. Ward ME, Toporsian M, Scott JA, et al. Hypoxia induces a functionally significant and translationally efficient neuronal NO synthase mRNA variant. J Clin Invest 2005;115:3128–3139. [PubMed: 16276418]
26. Benita Y, Kikuchi H, Smith AD, et al. An integrative genomics approach identifies Hypoxia Inducible Factor-1 (HIF-1)-target genes that form the core response to hypoxia. Nucleic Acids Res 2009;37:4587–4602. [PubMed: 19491311]
27. Puthanmadhom Narayanan S, O'Brien D, Sharma M, et al. Duodenal mucosal mitochondrial gene expression is associated with delayed gastric emptying in diabetic gastroenteropathy. JCI Insight 2021;6.
28. Luo L, Ambrozkiewicz MC, Benseler F, et al. Optimizing Nervous System-Specific Gene Targeting with Cre Driver Lines: Prevalence of Germline Recombination and Influencing Factors. Neuron 2020;106:37–65 e35. [PubMed: 32027825]

29. Colgan SP, Campbell EL, Kominsky DJ. Hypoxia and Mucosal Inflammation. Annu Rev Pathol 2016;11:77–100. [PubMed: 27193451]
30. Cipriani G, Gibbons SJ, Miller KE, et al. Change in Populations of Macrophages Promotes Development of Delayed Gastric Emptying in Mice. Gastroenterology 2018;154:2122–2136 e2112. [PubMed: 29501441]
31. Miller KE, Bajzer Z, Hein SS, et al. High temporal resolution gastric emptying breath tests in mice. Neurogastroenterol Motil 2018:e13333. [PubMed: 29575442]
32. Choi KM, Gibbons SJ, Nguyen TV, et al. Heme Oxygenase-1 Protects Interstitial Cells of Cajal From Oxidative Stress and Reverses Diabetic Gastroparesis. Gastroenterology 2008;135:2055–2064. [PubMed: 18926825]
33. Yang Y, Yu X, Zhang Y, et al. Hypoxia-inducible factor prolyl hydroxylase inhibitor roxadustat (FG-4592) protects against cisplatin-induced acute kidney injury. Clin Sci (Lond) 2018;132:825–838. [PubMed: 29581249]
34. Wang XJ, Burton DD, Breen-Lyles M, et al. Gastric accommodation influences proximal gastric and total gastric emptying in concurrent measurements conducted in healthy volunteers. Am J Physiol Gastrointest Liver Physiol 2021;320:G759–G767. [PubMed: 33719546]
35. May-Zhang AA, Tycksen E, Southard-Smith AN, et al. Combinatorial Transcriptional Profiling of Mouse and Human Enteric Neurons Identifies Shared and Disparate Subtypes In Situ. Gastroenterology 2021;160:755–770 e726. [PubMed: 33010250]
36. Morarach K, Mikhailova A, Knoflach V, et al. Diversification of molecularly defined myenteric neuron classes revealed by single-cell RNA sequencing. Nat Neurosci 2021;24:34–46. [PubMed: 33288908]
37. Amano T, Richelson E, Nirenberg M. Neurotransmitter synthesis by neuroblastoma clones (neuroblast differentiation-cell culture-choline acetyltransferase-acetylcholinesterase-tyrosine hydroxylase-axons-dendrites). Proc Natl Acad Sci U S A 1972;69:258–263. [PubMed: 4400294]
38. Anitha M, Joseph I, Ding X, et al. Characterization of fetal and postnatal enteric neuronal cell lines with improvement in intestinal neural function. Gastroenterology 2008;134:1424–1435. [PubMed: 18471518]
39. Phatnani HP, Greenleaf AL. Phosphorylation and functions of the RNA polymerase II CTD. Genes Dev 2006;20:2922–2936. [PubMed: 17079683]
40. Adelman K, Lis JT. Promoter-proximal pausing of RNA polymerase II: emerging roles in metazoans. Nat Rev Genet 2012;13:720–731. [PubMed: 22986266]
41. Yang Y, Lu H, Chen C, et al. HIF-1 Interacts with TRIM28 and DNA-PK to release paused RNA polymerase II and activate target gene transcription in response to hypoxia. Nat Commun 2022;13:316. [PubMed: 35031618]
42. Imakaev M, Fudenberg G, McCord RP, et al. Iterative correction of Hi-C data reveals hallmarks of chromosome organization. Nat Methods 2012;9:999–1003. [PubMed: 22941365]
43. Rao SS, Huntley MH, Durand NC, et al. A 3D map of the human genome at kilobase resolution reveals principles of chromatin looping. Cell 2014;159:1665–1680. [PubMed: 25497547]
44. Guo Y, Xu Q, Canzio D, et al. CRISPR Inversion of CTCF Sites Alters Genome Topology and Enhancer/Promoter Function. Cell 2015;162:900–910. [PubMed: 26276636]
45. Tang Z, Luo OJ, Li X, et al. CTCF-Mediated Human 3D Genome Architecture Reveals Chromatin Topology for Transcription. Cell 2015;163:1611–1627. [PubMed: 26686651]
46. Allan KC, Hu LR, Scavuzzo MA, et al. Non-canonical Targets of HIF1a Impair Oligodendrocyte Progenitor Cell Function. Cell Stem Cell 2021;28:257–272 e211. [PubMed: 33091368]
47. Stroka DM, Burkhardt T, Desbaillets I, et al. HIF-1 is expressed in normoxic tissue and displays an organ-specific regulation under systemic hypoxia. FASEB J 2001;15:2445–2453. [PubMed: 11689469]
48. Almeida AS, Figueiredo-Pereira C, Vieira HL. Carbon monoxide and mitochondria-modulation of cell metabolism, redox response and cell death. Front Physiol 2015;6:33. [PubMed: 25709582]
49. Ordog T, Takayama I, Cheung WK, et al. Remodeling of networks of interstitial cells of Cajal in a murine model of diabetic gastroparesis. Diabetes 2000;49:1731–1739. [PubMed: 11016458]
50. Choi KM, Gibbons SJ, Roeder JL, et al. Regulation of interstitial cells of Cajal in the mouse gastric body by neuronal nitric oxide. Neurogastroenterol Motil 2007;19:585–595. [PubMed: 17593140]

What You Need to Know

BACKGROUND AND CONTEXT:

Neuronal nitric oxide synthase contributes to the pathogenesis of gastroparesis. So far, measures to stimulate nitrergic signaling have been ineffective, necessitating alternative approaches.

NEW FINDINGS:

Hypoxia-inducible factor 1α (HIF1A) stimulated neuronal nitric oxide synthase gene transcription by binding and activating proximal and distal regulatory elements and by modifying 3-dimensional chromatin topology. Pharmacological stabilization of this protein with FG-4592/roxadustat, a drug approved for human use, reversed gastroparesis in diabetic mice.

LIMITATIONS:

Roxadustat upregulates nitric oxide synthase levels but does not ensure optimal functioning of this protein. Future studies will examine whether roxadustat can alleviate gastroparesis in patients.

CLINICAL RESEARCH RELEVANCE:

Reduced HIF1A resulting from mitochondrial dysfunction may contribute to gastric nitrergic neuropathy and diabetic gastroparesis in females. Pharmacological stabilization of HIF1A with a repurposed drug may be useful for treating diabetic gastroparesis in the future.

BASIC RESEARCH RELEVANCE:

Physiological intracellular hypoxia engenders HIF1A, which is required for normal transcription of the neuronal nitric oxide synthase gene. The newly recognized effects of HIF1A on chromosome topology may provide insights into physioxia- and ischemia-related organ function and the pathobiology of cancers.

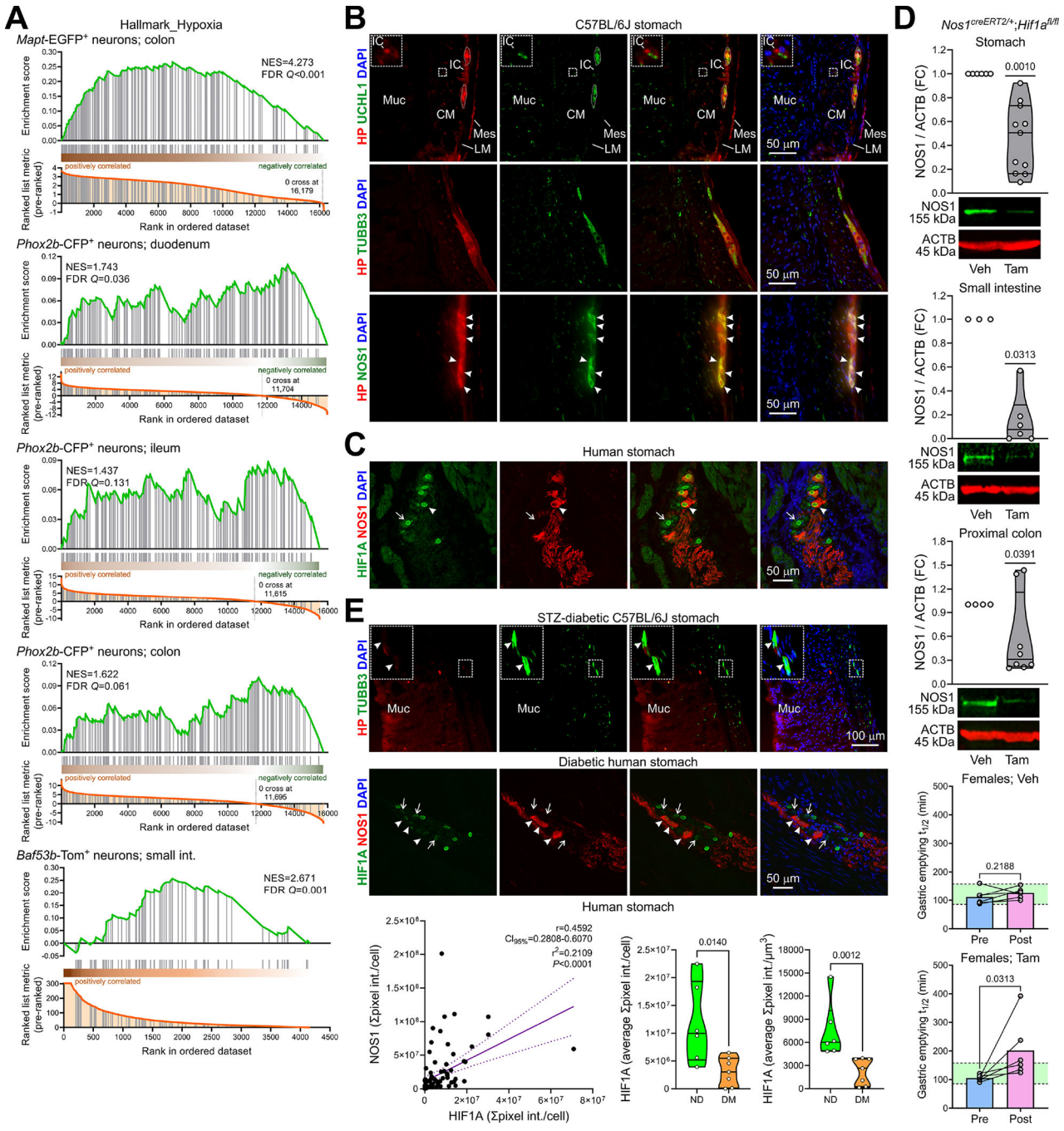

Figure 1. HIF1A from intracellular hypoxia is required for normal NOS1 levels in enteric neurons and for normal gastric emptying in female mice and is reduced in diabetes.

(*A*) Pre-ranked GSEA of hypoxia-related genes in enteric neurons. (*B*) Wide-field images of cryosections from nondiabetic mouse stomachs (n=2) showing Hypoxyprobe™ (HP)$^+$ cells. UCHL1, TUBB3, NOS1: neuronal markers. DAPI, 4',6-diamidino-2-phenylindole. IC, interstitial cells; Muc, mucosa; CM, circular muscle; LM, longitudinal muscle; Mes, mesothelial cells. Inset: enlargement of the outlined area showing a hypoxic IC adjacent to a nerve fiber. Dotted lines: enteric ganglia. Arrowheads: hypoxic NOS1$^+$ neurons. (*C*) Confocal images of cryosections from 4 nondiabetic patients showing predominantly nuclear

HIF1A (antibody: Thermo Fisher 700505) in $NOS1^+$ (arrowhead) and $NOS1^-$ (arrow) neurons. (*D*) Top panels: Reduction of NOS1 by genomic deletion of *Hif1a* in tamoxifen (Tam) vs. vehicle (Veh)-treated $Nos1^{creERT2/+};Hif1a^{fl/fl}$ mice (n_{Veh}=6, 3, 4; n_{Tam}=11, 6, 8). *P*, Wilcoxon signed rank tests. Bottom panels: Increase in GE $t_{1/2}$ by genomic deletion of *Hif1a* in female mice (n=6/group). Green area: strain- and sex-specific normal range. *P*, ratio-paired *t* tests. (*E*) Top: Wide-field images of cryosections from 2 STZ-diabetic mouse stomachs. Note reduced HP in $TUBB3^+$ enteric neurons (outlined area enlarged in the inset) and preserved HP in the luminal epithelium. Middle: Confocal images of cryosections from 4 diabetic patients showing reduced HIF1A (Thermo Fisher 700505) in $NOS1^+$ (arrowhead) and $NOS1^-$ (arrow) neurons. Bottom left: Direct linear relationship between HIF1A and NOS1 immunofluorescence in nitrergic neurons of 6 nondiabetic (n=37) and 7 diabetic patients (n=55). $CI_{95\%}$, 95% confidence interval. *P* is from linear regression and Pearson correlation. Right: HIF1A immunofluorescence/cell and immunofluorescence concentration were reduced in nitrergic neurons of the diabetic (DM) vs. nondiabetic (ND) patients. *P*, Mann-Whitney tests.

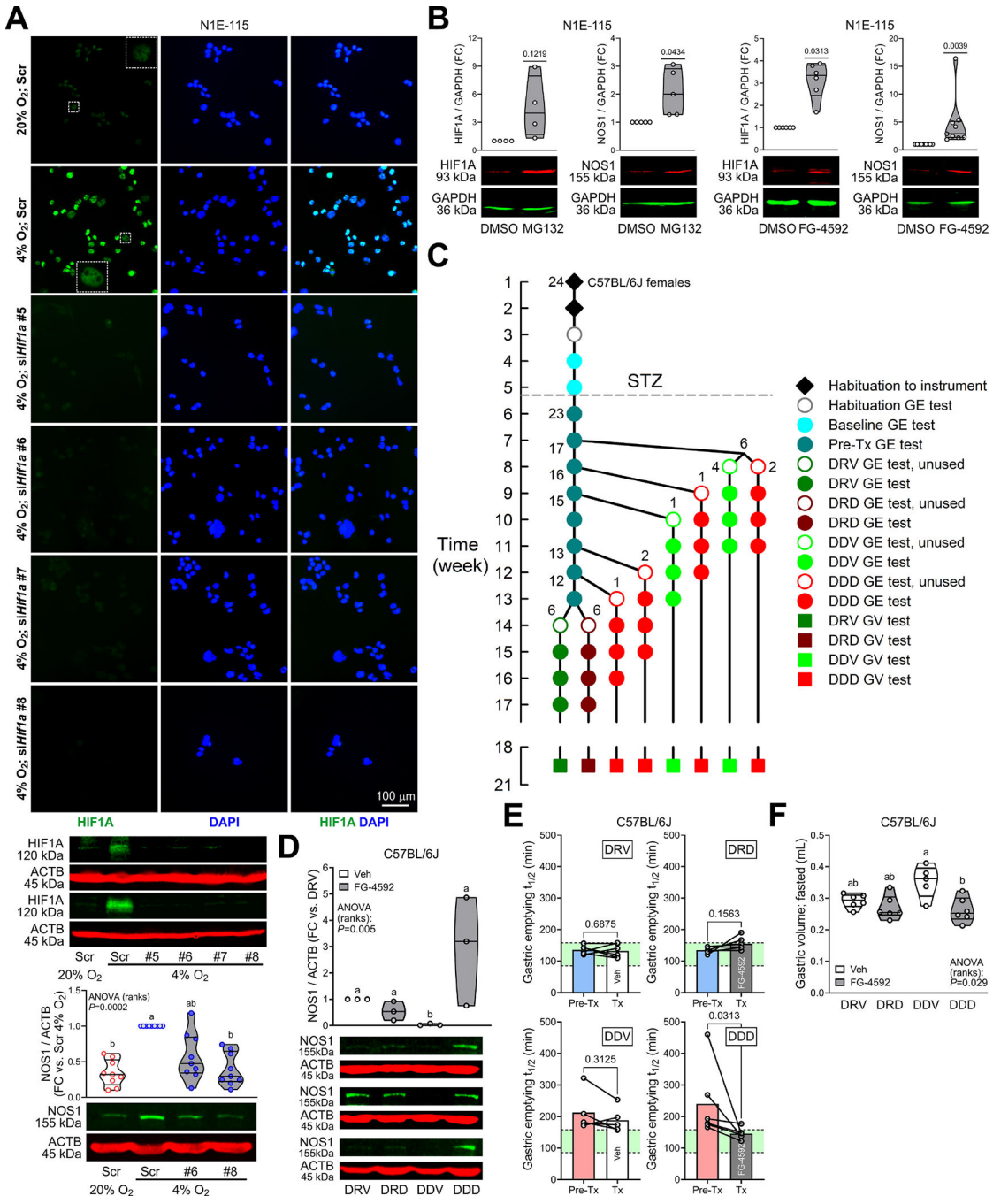

Figure 2. HIF1A stabilization restores NOS1 and reverses diabetic gastroparesis.

(*A*) Top and middle: Validation of *Hif1a* knockdown in N1E-115 cells by HIF1A immunofluorescence and immunoblotting (HIF1A antibody: Cell Signaling Technology #36169). Top: Wide-field images from 2 experiments. Scr, scrambled. Insets are enlargements of the outlined areas. Bottom: Effects of *Hif1a* knockdown on 4% O_2-induced upregulation of NOS1 protein (n=9). *P*, Kruskal-Wallis ANOVA on ranks. Groups not sharing the same superscript are different by Dunn's test. (*B*) Upregulation of HIF1A (Novus Biologicals NB100–134) and NOS1 protein by HIF1A stabilization with the

proteasome inhibitor MG132 (10μM, 4h) or the PHD inhibitor FG-4592 (20μM, 2 days) (HIF1A: $n_{MG132/Veh}$=4, $n_{FG-4592/Veh}$=6; NOS1: $n_{MG132/Veh}$=5; $n_{FG-4592/Veh}$=9). *P*, one sample *t* or Wilcoxon signed rank tests. NOS1 was upregulated even relative to the HIF1A target GAPDH. (*C*) Design of longitudinal GE study. One mouse did not develop diabetes. DRV, diabetic, resistant to GP, Veh-treated (n=6); DRD, diabetic, resistant to GP, FG-4592-treated (n=6); DDV, diabetic, delayed GE, Veh-treated (n=5); DDD, diabetic, delayed GE, FG-4592-treated (n=6). (*D*) Upregulation of NOS1 in GP mouse gastric corpus+antrum tunica muscularis by FG-4592 (n=3). *P*, Kruskal-Wallis ANOVA on ranks. Groups not sharing the same superscript are different by Tukey's test. (*E*) Significant reduction of GE $t_{1/2}$ from pretreatment values in GP mice treated with FG-4592 (DDD) but not in Veh-treated animals (DDV). GE $t_{1/2}$ did not change significantly in the non-GP mice (DRV, DRD). Green area: strain- and sex-specific normal range. *P*, Wilcoxon matched-pairs signed rank tests. (*F*) Normalization of fasting GVs by FG-4592. *P*, Kruskal-Wallis ANOVA on ranks. Groups not sharing the same superscript are different by Dunn's test.

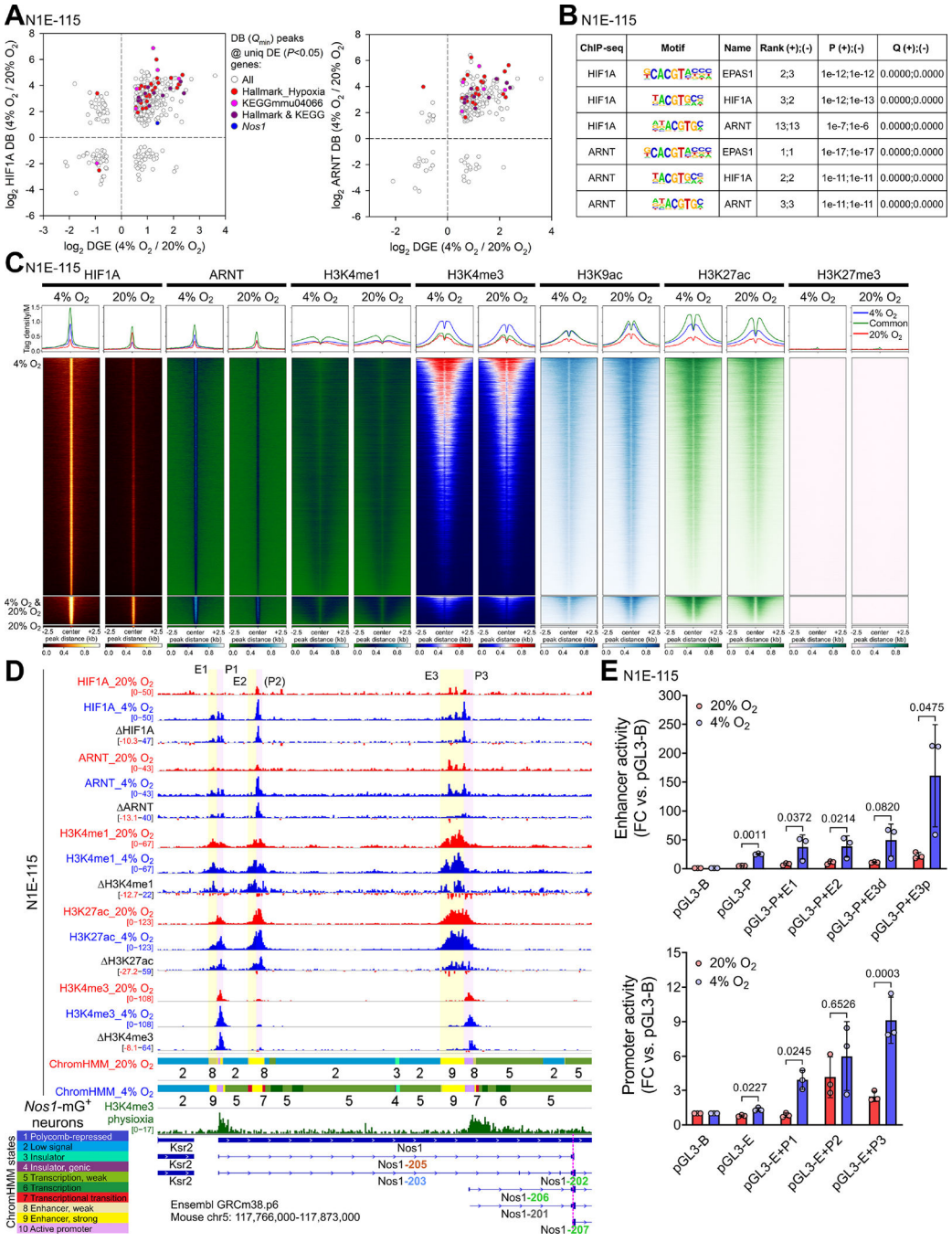

Figure 3. Hypoxia approximating physioxia increases HIF1A and ARNT binding to *cis*-regulatory elements of the *Nos1* locus.

(*A*) Correlation between differential binding (DB; FDR Q<0.1) of HIF1A and ARNT within peaks with the lowest FDR Q value among the peaks assigned to the same gene and differential gene expression (DE; P<0.05) in N1E-115 cells cultured for 3 days at 4% or 20% O_2. (*B*) Motifs within the HIF1A and ARNT peaks assigned to KEGG mmu04066 genes. (*C*) Heatmaps and average tag density plots of ChIP-seq data aligned to the centers of HIF1A peaks±2.5 kb are shown for HIF1A peaks unique to cells cultured at 4% O_2 (blue lines, top heatmap panels) or 20% O_2 (red lines, bottom heatmap panels) or common to cells

cultured at 4% or 20% O_2 (green lines, middle heatmap panels). (*D*) Binding profiles of HIF1A, ARNT, and key histone marks in the Ensembl GRCm38.p6 *Nos1* locus of N1E-115 cells cultured at 20% (red tracks) or 4% O_2 (blue) for 3 days. Aggregate and subtracted (4% O_2−20% O_2) occupancy data from two replicates are displayed. Colored ribbons: epigenetic states discovered by ChromHMM (10-state model). Green track: H3K4me3 in FACS-isolated *Nos1*-mG$^+$ enteric neurons. (*E*) Activities of the indicated candidate *Nos1 cis*-regulatory elements cloned into the pGL3-Promoter (pGL3-P; top) or the pGL3-Enhancer (pGL3-E; bottom) vectors vs. the pGL3-Basic (pGL3-B) plasmid. The E3 putative enhancer was separated into a *Nos1*-distal (E3d) and *Nos1*-proximal (E3p) fragment. *P*, ratio-paired *t* tests.

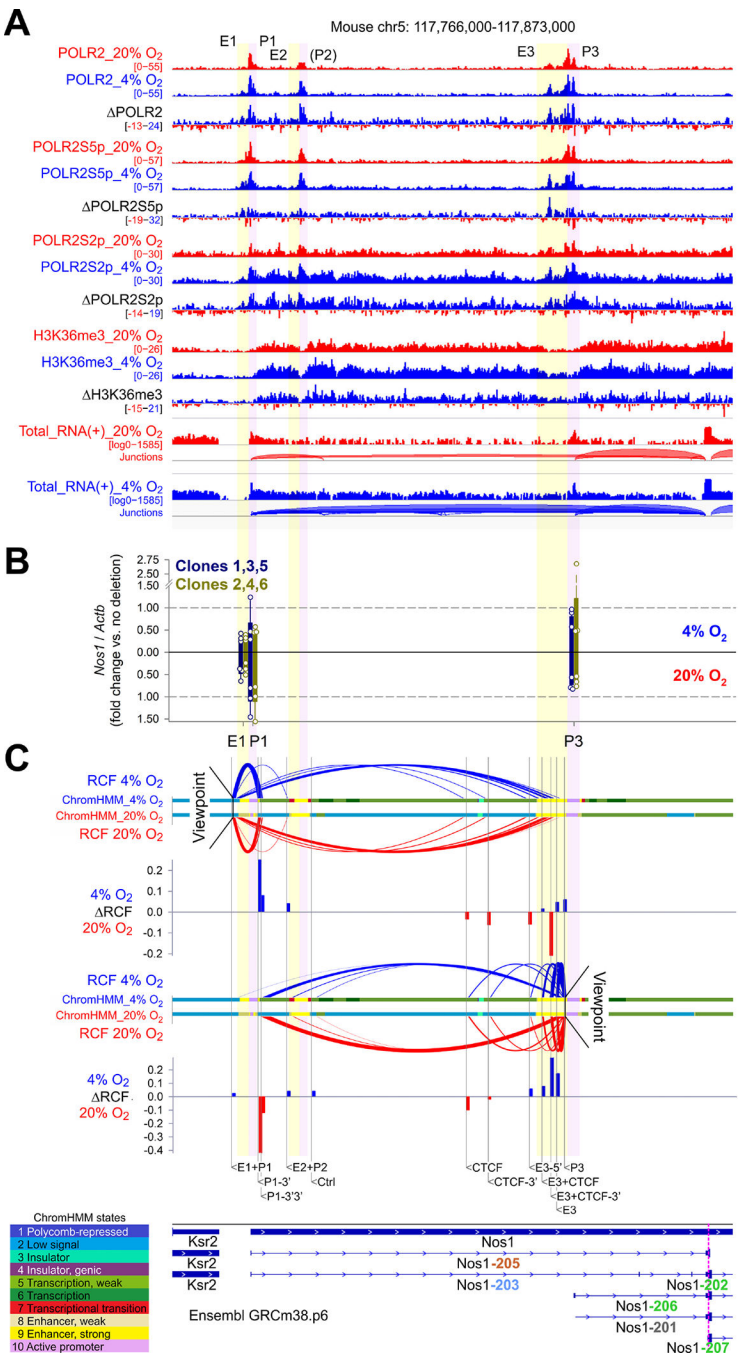

Figure 4. HIF1A controls *Nos1* transcription through multiple *cis*-regulatory elements of the *Nos1* locus.

(*A*) ChIP-seq and total RNA-seq (+ strand) profiles in the Ensembl GRCm38.p6 *Nos1* locus of N1E-115 cells cultured at 20% O_2 (red) or 4% O_2 (blue) for 3 days. Aggregate data from 2 (ChIP-seq) or 3 (RNA-seq) replicates and subtracted (4% O_2−20% O_2) data are displayed. (*B*) *Nos1* expression in N1E-115 cells bearing CRISPR-Cas9 deletions in E1, P1, and P3 (two clones/position, n=3 cultures/clone). Mean±SD data from cells cultured at 4% (upright) and 20% O_2 (inverted) are shown. (*C*) Enhancer-promoter loops detected by 3C using *Nco*I. qPCR data from 3 experiments were expressed relative to genomic DNA representing

the same locus expressed in bacterial artificial chromosome (BAC). BAC-normalized data were scaled to a range of 0–1 across the loci tested to compare data obtained at 4% O_2 (upright) and 20% O_2 (inverted). RCF, relative crosslinking frequency (scaled $2^{\Delta C}T$ vs. BAC). The colored ribbons identify epigenetic states discovered by ChromHMM using a 10-state model. Bar plots show ΔRCF values (4% O_2−20% O_2).

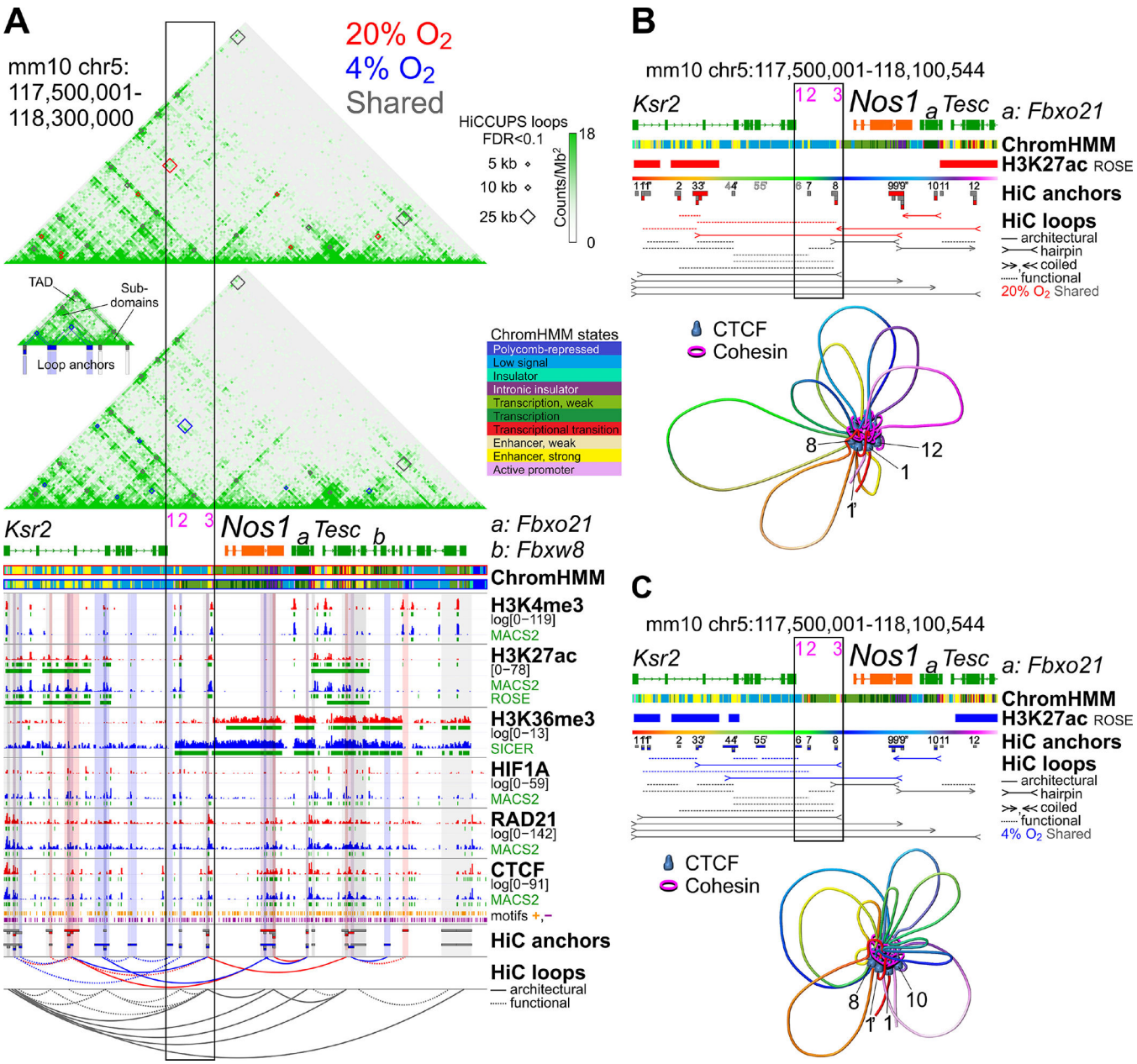

Figure 5. HIF1A binds remote super-enhancers that interact with *cis*-regulatory elements of the *Nos1* locus in a pO_2-dependent manner.

(*A*) Upper panel: HiC heatmaps of the TAD containing *Nos1* in N1E-115 cells cultured at 20% O_2 or 4% O_2 for 3 days. Chromosome loops detected at 5-, 10-, and 25-b resolution are displayed as red (loops unique to 20% O_2), blue (loops unique to 4% O_2), and gray diamonds (loops detected at both 20% and 4% O_2). Lower panel: ChromHMM and ChIP-seq tracks. Anchors and unscaled arc plots are color-coded as above. CTCF motif orientations are from ref.[44] Solid and dashed lines: architectural and functional/transient loops, respectively. Black rectangle: *cis*-regulatory elements of the Ensembl *Nos1* locus. (*B*) Upper panel: loops in N1E-115 cells cultured at 20% O_2. Arrows: CTCF motif orientations permissive to architectural loop formation (convergent, left tandem, right tandem). Dashed

lines without arrows: functional/transient loops. Lower panel: 3D chromatin structure of the locus inferred from the loop data. Numbered CTCF molecules correspond to the numbering of loop anchors in the upper panel. (*C*) Loops, and proposed chromosome conformation in N1E-115 cells cultured at 4% O_2. See legend to panel *B*.

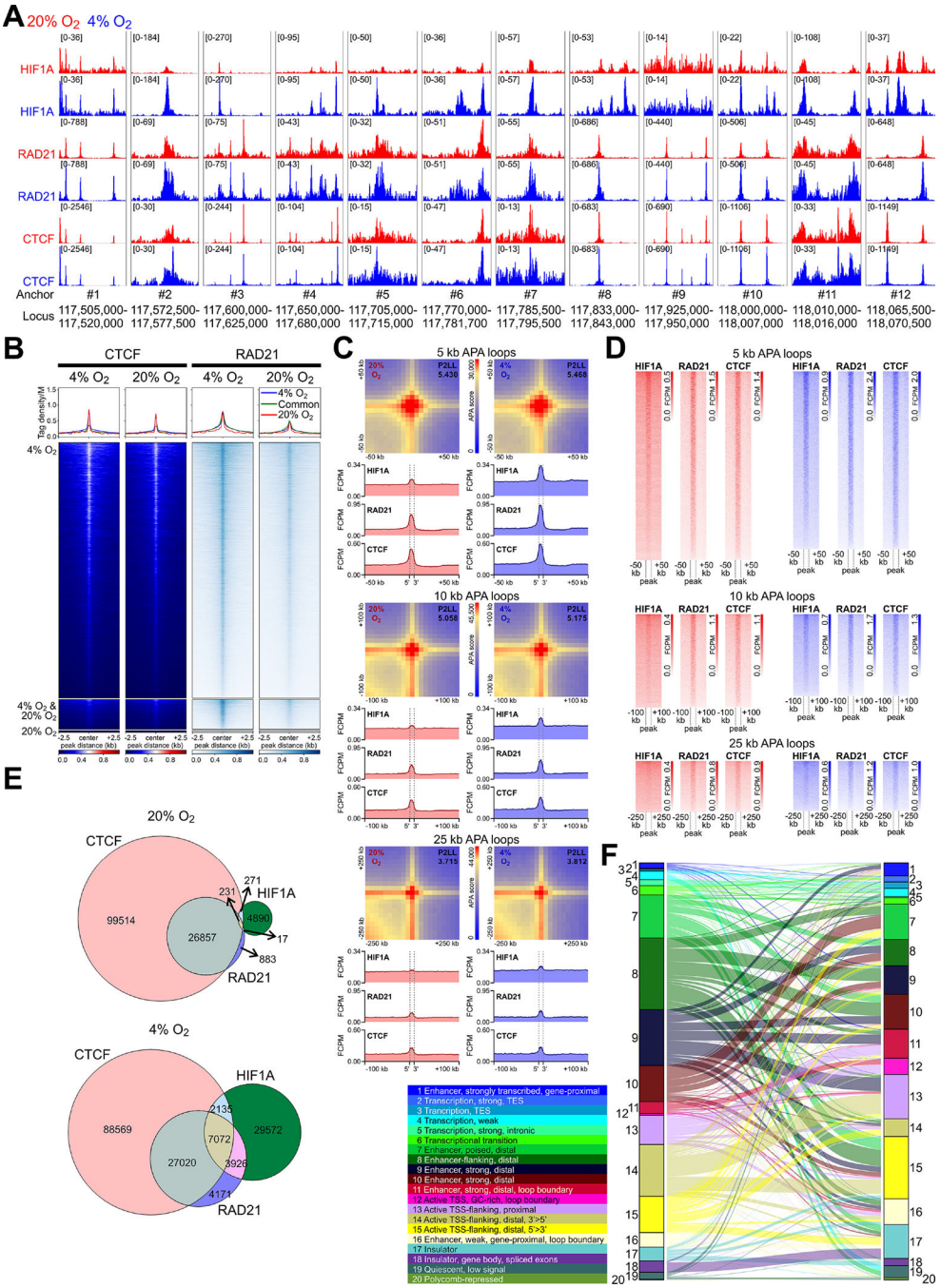

Figure 6. HIF1A alters chromosome topology genomewide.

(*A*) HIF1A, RAD21, and CTCF binding (aggregate data from 2 replicates/condition) in N1E-115 cells within 12 clusters of HiC loop anchors identified in Figure 5. (*B*) Heatmaps and average tag density plots of CTCF and RAD21 ChIP-seq data aligned to the centers of HIF1A peaks±2.5 kb (see in Figure 3C) are shown for HIF1A peaks unique to cells cultured at 4% O_2 (blue lines, top heatmap panels) or 20% O_2 (red lines, bottom heatmap panels) or common to cells maintained at 4% O_2 or 20% O_2 (green lines, middle heatmap panels). (*C*) Heatmaps of standard APA results obtained at 5-, 10-, and 25-kb resolution. P2LL,

peak-to-lower-left-quadrant enrichment values. Below the APA plots, HIF1A, RAD21, and CTCF average tag density plots centered around all detected APA loop anchors are shown. Dashed vertical lines demarcate the central APA bins. (*D*) Heatmaps corresponding to the average tag density plots in *C*. (*E*) Venn diagrams showing overlaps of HIF1A, CTCF, and RAD21 peaks at 20% O_2 and 4% O_2. (*F*) Sankey plot showing chromatin state changes from 20% O_2 (left) to 4% O_2 (right) in N1E-115 cells. The colored ribbons show the relative frequencies of epigenetic states discovered by ChromHMM using a 20-state model.

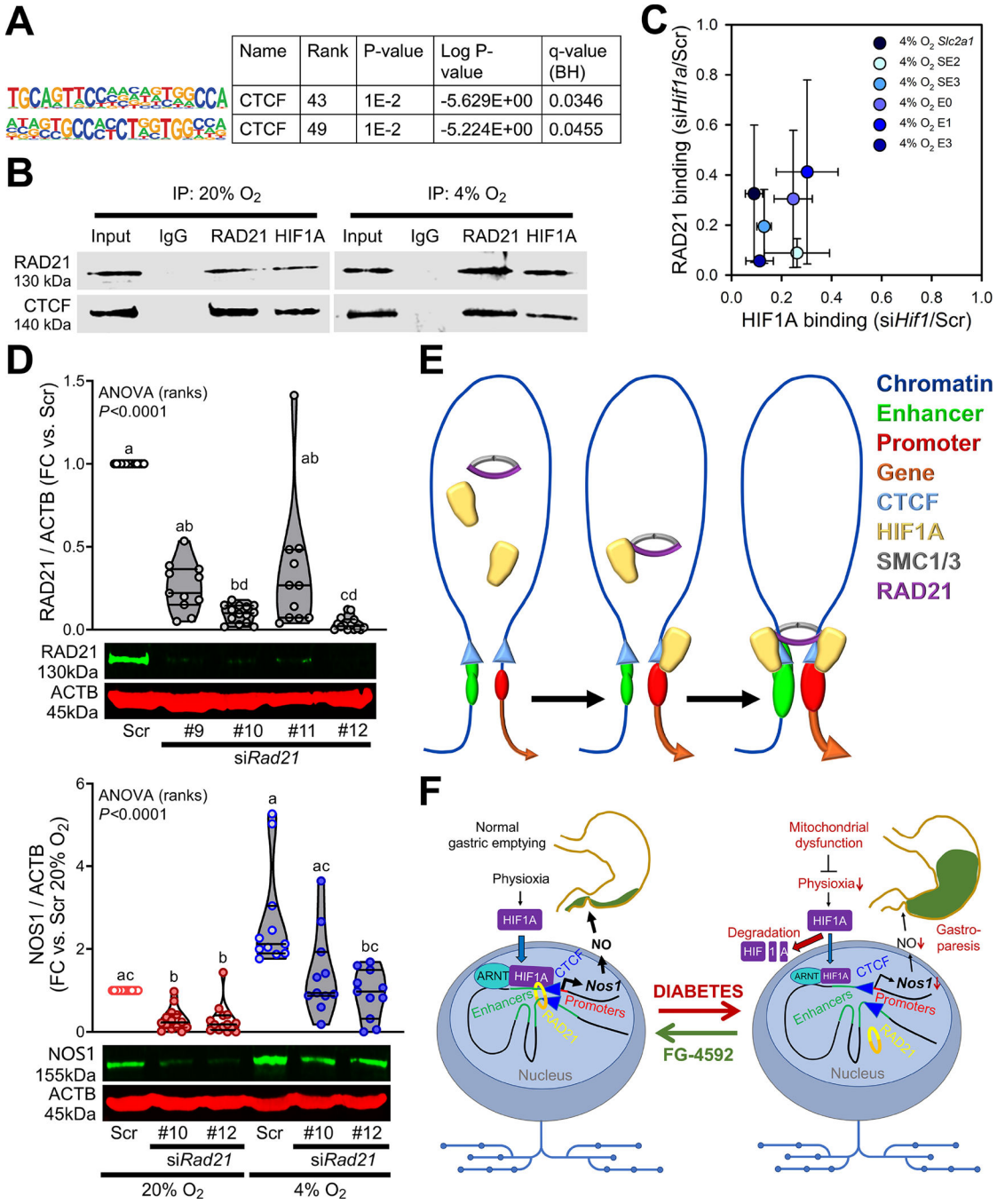

Figure 7. HIF1A recruits RAD21 to CTCF-bound sites to upregulate NOS1.

(*A*) Enrichment of known CTCF motifs in HIF1A-bound *cis*-regulatory elements of the *Nos1* TAD in N1E-115 cells. (*B*) Co-immunoprecipitation of RAD21 and CTCF with RAD21 and HIF1A. Representative immunoblots from 3 (RAD21) or 2 (CTCF) experiments. (*C*) Concordant reduction in HIF1A and RAD21 binding in the promoter of the canonical HIF1A target *Slc2a1* gene and key HIF1A-bound SEs and enhancers of the sub-TAD containing *Nos1* in HIF1A-silenced N1E-115 cells cultured at 4% O_2. The loci targeted for analysis are indicated by pink bars in Supplementary Figure 10D

and a pink vertical line in Supplementary Figure 7A. (*D*) Top: Silencing efficiencies of 4 siRNAs targeting *Rad21*. n_{Scr}=14, $n_{\#9}$=11, $n_{\#10}$=14, $n_{\#11}$=11, $n_{\#12}$=14. *P*, Kruskal-Wallis one-way ANOVA. Groups not sharing the same superscript are different by Dunn's test. Bottom: Effects of *Rad21* knockdown using the two most efficacious siRNAs on NOS1 protein in N1E-115 cells. $n_{Scr;20\%}$=14, $n_{\#10;20\%}$=14, $n_{\#12;20\%}$=14, $n_{Scr;4\%}$=11, n#10;4%=11, $n_{\#12;4\%}$=11. *P*, Kruskal-Wallis one-way ANOVA. Groups not sharing the same superscript are different by Dunn's test. (*E*) Schematic illustration showing the formation of architectural enhancer-promoter loops triggered by HIF1A recruitment of RAD21 to CTCF-bound sites. (*F*) Overview of the proposed main roles of HIF1A in gastroparesis.